Universität des Saarlandes

Fachrichtung 6.1 – Mathematik

Preprint Nr. 104

Curvature-Driven PDE Methods for Matrix-Valued Images

Christian Feddern, Joachim Weickert,
Bernhard Burgeth and Martin Welk

Saarbrücken 2004

Fachrichtung 6.1 – Mathematik
Universität des Saarlandes

Preprint No. 104
submitted: 13th April, 2004

Curvature-Driven PDE Methods for Matrix-Valued Images

Christian Feddern
Saarland University
Faculty of Mathematics and Computer Science
Building 27.1, P.O. Box 15 11 50
66041 Saarbrücken
Germany
feddern@mia.uni-saarland.de

Joachim Weickert
Saarland University
Faculty of Mathematics and Computer Science
Building 27.1, P.O. Box 15 11 50
66041 Saarbrücken
Germany
weickert@mia.uni-saarland.de

Bernhard Burgeth
Saarland University
Faculty of Mathematics and Computer Science
Building 27.1, P.O. Box 15 11 50
66041 Saarbrücken
Germany
burgeth@mia.uni-saarland.de

Martin Welk
Saarland University
Faculty of Mathematics and Computer Science
Building 27.1, P.O. Box 15 11 50
66041 Saarbrücken
Germany
welk@mia.uni-saarland.de

Edited by
FR 6.1 – Mathematik
Universität des Saarlandes
Postfach 15 11 50
66041 Saarbrücken
Germany

Fax: + 49 681 302 4443
e-Mail: preprint@math.uni-sb.de
WWW: http://www.math.uni-sb.de/

Abstract

Matrix-valued data sets arise in a number of applications including diffusion tensor magnetic resonance imaging (DT-MRI) and physical measurements of anisotropic behaviour. Consequently, there arises the need to filter and segment such tensor fields. In order to detect edge-like structures in tensor fields, we first generalise Di Zenzo's concept of a structure tensor for vector-valued images to tensor-valued data. This structure tensor allows us to extend scalar-valued mean curvature motion and self-snakes to the tensor setting. We present both two-dimensional and three-dimensional formulations, and we prove that these filters maintain positive semidefiniteness if the initial matrix data are positive semidefinite. We give an interpretation of tensorial mean curvature motion as a process for which the corresponding curve evolution of each generalised level line is the gradient descent of its total length. Moreover, we propose a geodesic active contour model for segmenting tensor fields and interpret it as a minimiser of a suitable energy functional with a metric induced by the tensor image. Since tensorial active contours incorporate information from all channels, they give a contour representation that is highly robust under noise. Experiments on three-dimensional DT-MRI data and an indefinite tensor field from fluid dynamics show that the proposed methods inherit the essential properties of their scalar-valued counterparts.

1 Introduction

Curvature-based partial differential equations (PDEs) play an important role in image processing and computer vision. They include a number of interesting PDEs such as mean curvature motion [1], self-snakes [43] and geodesic active contours [8, 25]. Often it is helpful to study their behaviour by investigating the evolutions of the corresponding level lines. On one hand this links these techniques to level set methods [14, 35, 32, 33, 46], on the other hand one may interpret these evolutions as steepest descent strategies for minimising interesting energy functionals.
While curvature-based PDEs have been extended in various ways to higher dimensions, surfaces and vector-valued data (see e.g. [27, 33, 43], there are hardly any attempts so far to use them for processing tensor-valued data sets. However, such data sets are becoming increasingly important for three reasons:

1. Novel medical imaging techniques such as diffusion tensor magnetic resonance imaging (DT-MRI) have been introduced [38]. DT-MRI is a

3-D imaging method that yields a diffusion tensor in each voxel. This diffusion tensor describes the diffusive behaviour of water molecules in the tissue. It can be represented by a positive semidefinite 3×3 matrix in each voxel.

2. Tensors have shown their use as a general tool in image analysis, segmentation and grouping [19, 31]. This also includes widespread applications of the so-called structure tensor in fields ranging from motion analysis to texture segmentation; see e.g. [2, 41].

3. A number of scientific applications require the visualisation and processing of tensor fields [47]. The tensor concept is a common physical description of anisotropic behaviour, especially in solid mechanics and civil engineering (e.g. stress-strain relationships, inertia tensors, diffusion tensors, permittivity tensors).

The search for good smoothing techniques for DT-MRI data and related tensor fields is a very recent research area. Several authors have addressed this problem by smoothing derived expressions such as the eigenvalues and eigenvectors of the diffusion tensor [12, 39, 48] or rotationally invariant scalar-valued expressions [36, 57]. Also for fiber tracking applications, most techniques work on scalar- or vector-valued data [6, 50]. Some image processing methods that work directly on the tensor components use linear [55] or nonlinear [22] techniques that filter all channels *independently*, thus performing scalar-valued filtering again. Nonlinear variational methods for matrix-valued filtering with channel coupling have been proposed both in the isotropic [48] and in the anisotropic setting [53]. Related nonlinear diffusion methods for tensor-valued data have led to the notion of a nonlinear structure tensor [53] that has been used for optic flow estimation [4], texture discrimination and tracking [3]. Recently also tensorial generalisations of median filtering [54], morphological methods [5], and Mumford–Shah segmentations [51] have been studied. We are, however, not aware of any attempts to generalise curvature-based PDEs to the tensor setting.

The goal of the present paper is to introduce three curvature-based PDEs for analysing and processing two- and three-dimensional tensor fields. They can be regarded as tensor-valued extensions of mean curvature motion, self-snakes and geodesic active contours. The key ingredient for this generalisation is the use of a structure tensor for matrix-valued data.

Our paper is organised as follows. In Section 2 we introduce the generalised structure tensor for matrix fields. It is then used in Section 3 for designing a 2-D mean curvature type evolution of tensor-valued data. In this section we also derive a variational formulation of tensorial mean curvature motion that

is in accordance with its scalar counterpart. Modifying tensor-valued mean curvature motion by a suitable edge stopping function leads us to tensor-valued self-snakes. They are discussed in Section 4. In Section 5, we use the self-snake model in order to derive geodesic active contour models for tensor fields. Three-dimensional extensions of mean curvature motion, self snakes and geodesic active contours are presented in Section 6, where we also prove that tensorial mean curvature motion preserves positive semidefiniteness of the input data. Algorithmic details are sketched in Section 7, and two- as well as three-dimensional experiments are presented in Section 8. The paper is concluded with a summary in Section 9.
A preliminary, shorter version of our paper has been presented at VLSM 2003 [16]. The present paper extends this work substantially: It derives three-dimensional results, it presents interpretations in terms of energy functionals that are minimised, and it shows additional experiments with indefinite tensor fields from fluid dynamics.

2 Structure Analysis of Tensor-Valued Data

In this section we generalise the concept of an image gradient to the tensor-valued setting. This may be regarded as a tensor extension of Di Zenzo's and Cumani's method for vector-valued data [15, 13].
Let us consider some 2×2 tensor image $(f_{i,j}(x,y))$ where the indices (i,j) specify the tensor channel. We would like to define an "edge direction" for such a matrix-valued function. In the case of some scalar-valued image $f(x,y)$, we would look for the direction v which is orthogonal to the gradient of a Gaussian-smoothed version of f:

$$0 = v^\top \nabla f_\sigma \tag{1}$$

where $f_\sigma := K_\sigma * f$ and K_σ denotes a Gaussian with standard deviation σ. Gaussian convolution makes the structure detection more robust against noise. The parameter σ is called *noise scale*.
In the general tensor-valued case, we cannot expect that all tensor channels yield the same edge direction. Therefore we proceed as follows. Let $f_{\sigma,i,j}$ be a Gaussian-smoothed version of $f_{i,j}$. Then we define the edge direction as the unit vector v that minimises

$$\begin{aligned} E(v) &:= \sum_{i=1}^{2}\sum_{j=1}^{2}(v^\top \nabla f_{\sigma,i,j})^2 \\ &= v^\top \Big(\sum_{i=1}^{2}\sum_{j=1}^{2} \nabla f_{\sigma,i,j} \nabla f_{\sigma,i,j}^\top\Big) v. \end{aligned} \tag{2}$$

This quadratic form is minimised, when v is eigenvector to the smallest eigenvalue of the *structure tensor*

$$J(\nabla f_\sigma) := \sum_{i=1}^{2}\sum_{j=1}^{2} \nabla f_{\sigma,i,j} \nabla f_{\sigma,i,j}^\top. \tag{3}$$

The trace of this matrix can be regarded as a tensor-valued generalisation of the squared gradient magnitude:

$$\mathrm{tr} J(\nabla f_\sigma) = \sum_{i=1}^{2}\sum_{j=1}^{2} |\nabla f_{\sigma,i,j}|^2. \tag{4}$$

The matrix $J(\nabla f_\sigma)$ will enable us to generalise a number of curvature-based PDE methods to the tensor-valued setting. Indeed, extending the ideas in [11] to the matrix-valued case, one my even define level lines of matrix-valued images as the integral curves of the eigenvector directions to the smallest eigenvalue of $J(\nabla f_\sigma)$. Such an interpretation allows to relate the subsequent tensor-based methods to level set strategies.

3 Mean Curvature Motion

In this section we introduce a tensor-valued mean curvature motion. To this end, we first have to sketch some basic ideas behind scalar-valued mean curvature motion.
We start with the observation that the Laplacian of an isotropic linear diffusion model may be decomposed into two orthogonal directions $\xi \perp \nabla u$ and $\eta \parallel \nabla u$:

$$\begin{aligned} \partial_t u &= \partial_{xx} u + \partial_{yy} u & (5)\\ &= \partial_{\xi\xi} u + \partial_{\eta\eta} u & (6) \end{aligned}$$

where $\partial_{\xi\xi} u$ describes smoothing parallel to edges and $\partial_{\eta\eta} u$ smoothes perpendicular to edges. *Mean curvature motion (MCM)* uses an anisotropic variant of this smoothing process by permitting only smoothing along the level lines:

$$\partial_t u = \partial_{\xi\xi} u \tag{7}$$

This can be rewritten as

$$\partial_t u = |\nabla u| \ \mathrm{div} \left(\frac{\nabla u}{|\nabla u|} \right). \tag{8}$$

Alvarez *et al.* have used this evolution equation for denoising highly degraded images [1], and Kimia and Siddiqi have studied its scale-space properties [26]. It is well-known from the mathematical literature [17, 20, 23] that under MCM convex level lines remain convex, nonconvex ones become convex, and in finite time they vanish by shrinking to *circular points* (a point with a circle as limiting shape). Interestingly, mean curvature motion plays a similar role for morphology as linear diffusion does in the context of linear averaging. While iterated and suitably scaled convolutions with smoothing masks approximate linear diffusion filtering, it has been shown that iterated classic morphological operators such as median filtering are approximating MCM [21]. Similar approximation results can also be established in the vector-valued setting [9].

If we want to use a MCM-like evolution for processing tensor-valued data $(f_{i,j})$, it is natural to replace the second directional derivative $\partial_{\xi\xi} u$ in (7) by $\partial_{vv} u$, where v is the eigenvector to the smallest eigenvalue of the structure tensor $J(\nabla u)$. This leads us to the evolution

$$\partial_t u_{i,j} = \partial_{vv} u_{i,j}, \tag{9}$$

$$u_{i,j}(x, y, 0) = f_{i,j}(x, y) \tag{10}$$

for all tensor channels (i, j). Note that this process synchronises the smoothing direction in all channels. It may be regarded as a tensor-valued generalisation of the vector-valued mean curvature motion proposed by Chambolle [10] and its modifications by Sapiro and Ringach [44]. The synchronisation of channel smoothing is also a frequently used strategy in vector-valued diffusion filtering [18, 52, 29, 49].

Variational Formulation. It is well-known (see e.g. [43]) that MCM for scalar-valued images admits a variational formulation: If C is a closed level set curve of u, then $L(C) := \oint_C ds$ with the Euclidean metric $ds^2 = dx^2 + dy^2$ gives the Euclidean length of C. MCM then turns out to be a gradient descent for $L(C)$.

In order to formulate a similar statement in the tensor-valued case, two obstacles have to be overcome. Both result from the fact that the range of the image values is now of higher dimension than the image domain.

First, there are in general no level lines, i.e. lines in the image domain along which the image value is constant. However, in [11] Chung and Sapiro have introduced a concept of generalised level lines for vector-valued images which can easily be transferred to our tensor-valued setting. They define level lines as *lines of minimal change* of the image value. Each regular point of the image is traversed by one and only one level line, the direction of which is

given by the eigenvector for the smallest eigenvalue of the structure tensor $J(\nabla u)$. The so defined level lines share essential properties with level lines for scalar-valued functions. Most important, regular level lines are closed curves and have no crossings. We note that this concept is in perfect harmony with eq. (9) because it allows to describe MCM as smoothing along level lines, exactly like in the scalar case.

Second, even with a concept of level lines, it is not obvious how a curve evolution should correspond to a given image evolution. In general, the particular tensor values which are present in the image along a certain curve C at some time t will not be found in the image at another time t. A first idea that follows the spirit of the level-line concept introduced above is that the image (tensor) values of curve points moving with the curve should change *as little as possible* in time. To this end, the curve evolution $C(s,t)$ should be chosen such as to minimise $\|\partial_t u(C(t))\|$. Slightly modifying this idea, we consider the normal curve evolution $C = C(s,t)$ for which the expression

$$\|\partial_t u(C(s,t))\|^2 - \|\partial_t C(s,t)\|^2 \|\partial_s u(C(s,t))\|^2 + \frac{1}{2}\partial_t \|\partial_s u(C(s,t))\|^2 \quad (11)$$

becomes minimal where s is the arc-length parameter of C. Note that the second and third members of the sum tie the temporal constancy requirement ruling the curve evolution to the spatial constancy requirement defining level lines. The second member relaxes the temporal constancy at curve segments where the deviation from spatial constancy is high while the third member penalises or rewards deterioration or improvement of the spatial constancy in time. For a conventional level line evolution, with perfect spatial and temporal constancy, both summands vanish.

With these ingredients, the MCM evolution (9) is characterised as the image evolution for which the corresponding curve evolution of each level lines is the gradient descent for the total length of this level line.

To see this, we remark first that the curvature of a level line of the tensor-valued image u in the point (x,y) equals

$$\kappa(x,y) = \frac{\sum_{i,j} \partial_{vv} u_{i,j}\, \partial_z u_{i,j} + \sum_{i,j} \partial_{vz} u_{i,j}\, \partial_v u_{i,j}}{\sum_{i,j} (\partial_z u_{i,j})^2 - \sum_{i,j} (\partial_v u_{i,j})^2} \quad (12)$$

where v and z are tangential and normal unit vectors for the level line, i.e. eigenvectors for the smaller and larger eigenvalues of $J(\nabla u)$. The curvature flow for the level line C traversing (x,y) which is known (see e.g. [27]) to be the gradient descent flow for the Euclidean length of C, is exactly $C_t = \kappa \cdot z$. Assume now we have a tensor-valued image evolution $u_{i,j} = u_{i,j}(x,y,t)$ with $i,j \in \{1,2\}$. Assume again that a curve C with tangential vector v and

normal vector z traverses through (x, y). Then the normal flow of C that minimises (11) is given by $C_t = \tau z$ where τ satisfies

$$\partial_\tau \Big(\sum_{i,j} (\partial_z u_{i,j} \tau + \partial_t u_{i,j})^2 - \tau^2 \sum_{i,j} (\partial_v u_{i,j})^2 + \frac{1}{2} \tau \partial_z (\partial_v u_{i,j})^2 \Big) = 0 \qquad (13)$$

or

$$\tau \sum_{i,j} (\partial_z u_{i,j})^2 + \sum_{i,j} \partial_z u_{i,j} \partial_t u_{i,j} - \tau \sum_{i,j} (\partial_v u_{i,j})^2 + \sum_{i,j} (\partial_v u_{i,j} \partial_{vz} u_{i,j}) = 0. \quad (14)$$

Obviously $\tau = \kappa$ satisfies the last equation if and only if $u_t = u_{vv}$, i.e. if u evolves according to the MCM equation (9).

4 Self-Snakes

In [42], Sapiro has proposed a specific variant of MCM that is well-suited for image enhancement. This process which he names *self-snakes* introduces an edge-stopping function into mean curvature motion in order to prevent further shrinkage of the level lines once they have reached important image edges. In the scalar-valued setting, a self-snake $u(x, y, t)$ of some image $f(x, y)$ is generated by the evolution process

$$\partial_t u = |\nabla u| \operatorname{div} \left(g(|\nabla u|^2) \frac{\nabla u}{|\nabla u|} \right), \qquad (15)$$

$$u(x, y, 0) = f(x, y), \qquad (16)$$

where g is a decreasing function such as the Perona-Malik diffusivity [37]

$$g(|\nabla u|^2) := \frac{1}{1 + |\nabla u|^2 / \lambda^2}. \qquad (17)$$

In order to make self-snakes more robust under noise it is common to replace $g(|\nabla u|^2)$ by its Gaussian-regularised variant $g(|\nabla u_\sigma|^2)$. Self-snakes have been advocated as alternatives to nonlinear diffusion filters [56], they can be used for vector-valued images [42], and related processes have also been proposed for filtering 3-D images [40].
Using the product rule of differentiation, we may rewrite Equation (15) as

$$\partial_t u = g(|\nabla u_\sigma|^2) \, \partial_{\xi\xi} u + \nabla^\top (g(|\nabla u_\sigma|^2)) \, \nabla u. \qquad (18)$$

This formulation suggests a straightforward generalisation to the tensor-valued setting. All we have to do is to replace $|\nabla u_\sigma|^2$ by $\mathrm{tr} J(\nabla u_\sigma)$, and

$\partial_{\xi\xi}$ by ∂_{vv} where v is the eigenvector to the smallest eigenvalue of $J(\nabla u)$. This leads us to the following tensor-valued evolution:

$$\begin{aligned} \partial_t u_{i,j} &= g(\mathrm{tr} J(\nabla u_\sigma))\, \partial_{vv} u_{i,j} + \nabla^\top (g(\mathrm{tr} J(\nabla u_\sigma)))\, \nabla u_{i,j}, \quad (19) \\ u_{i,j}(x,y,0) &= f_{i,j}(x,y). \quad (20) \end{aligned}$$

We observe that the main difference to tensor-valued MCM consists of the additional term $\nabla^\top (g(\mathrm{tr} J(\nabla u_\sigma)))\, \nabla u_{i,j}$. It can be regarded as a shock filter [28, 34] that is responsible for the edge-enhancing properties of self-snakes.

5 Active Contour Models

Active contours [24] play an important role in interactive image segmentation, in particular for medical applications. The underlying idea is that the user specifies an initial guess of an interesting contour (organ, tumour, ...). Then this contour is moved by image-driven forces to the edges of the object in question.

So-called geodesic active contour models [8, 25] achieve this by applying a specific kind of level set ideas. They may be regarded as extensions of the implicit snake models in [7, 30]. In its simplest form, a geodesic active contour model consists of the following steps. One embeds the user-specified initial curve $C_0(s)$ as a zero level curve into a function $f(x, y)$, for instance by using the distance transformation. Then f is evolved under a PDE which includes knowledge about the original image h:

$$\begin{aligned} \partial_t u &= |\nabla u|\, \mathrm{div} \left(g(|\nabla h_\sigma|^2)\, \frac{\nabla u}{|\nabla u|} \right), \quad (21) \\ u(x,y,0) &= f(x,y), \quad (22) \end{aligned}$$

where g inhibits evolution at edges of f. One may choose decreasing functions such as the Perona–Malik diffusivity (17). Experiments indicate that, in general, (21) will have nontrivial steady states. The evolution is stopped at some time T, when the process does hardly alter anymore, and the final contour C is extracted as the zero level curve of $u(x, T)$.

To extend this idea to tensor valued data $h_{i,j}$, we propose to use $\mathrm{tr}(J(\nabla h_\sigma))$ as argument of the stopping function g.

$$\partial_t u = |\nabla u|\, \mathrm{div} \left(g(\mathrm{tr} J(\nabla h_\sigma))\, \frac{\nabla u}{|\nabla u|} \right). \quad (23)$$

Note that, in contrast to the processes in the previous section, this equation is still scalar-valued, since the goal is to find a contour that segments all

channels simultaneously. The active contour evolution for this process may be rewritten as

$$\begin{aligned} \partial_t u &= g(\mathrm{tr} J(\nabla h_\sigma))\, \partial_{\xi\xi} u + \nabla^\top (g(\mathrm{tr} J(\nabla h_\sigma)))\, \nabla u, && (24) \\ u(x,y,0) &= f(x,y). && (25) \end{aligned}$$

Since a tensor-valued image involves more channels than a scalar-valued one, we can expect that this additional information stabilises the process when noise is present. Our experiments in Section 7 will confirm this expectation. The geodesic active contour model also allows a description in terms of a variational problem. Since u is scalar-valued, the transfer from the case of scalar images works straightforward.
We equip the image domain with the metric defined by

$$ds^2 = g(\mathrm{tr}(\nabla h_\sigma))\, (dx^2 + dy^2) \tag{26}$$

where $dx^2 + dy^2$ is the Euclidean metric. The length of a closed contour C w.r.t. this metric reads

$$L(C) = \oint_C ds = \oint_C g(\mathrm{tr}(\nabla h_\sigma))\, (dx^2 + dy^2)^{1/2}. \tag{27}$$

Then the active contour evolution is a gradient descent for $L(C)$ which converges to a contour of minimal length, i.e. a geodesic in the metric ds. For scalar-valued images this has been proven in [43]. Since the proof does not rely on any property of g specific to scalar-valued images, it transfers verbatim to the tensor-valued setting.

6 Images with 3×3-Tensors

All previous discussions are based on tensor fields with 2×2 matrices over a two-dimensional image domain. However, many applications such as DT-MRI involve 3×3 tensor fields over a three-dimensional image domain. Let us now investigate how our results can be transferred to this situation.

Structure Tensor. The notion of structure tensor defined in (3) can be extended without any difficulties to the case of 3×3 tensor images:

$$J(\nabla f_\sigma) := \sum_{i=1}^{3} \sum_{j=1}^{3} \nabla f_{\sigma,i,j} \nabla f_{\sigma,i,j}^\top \tag{28}$$

where $f = f(x, y, z)$ and $\nabla = (\partial_x, \partial_y, \partial_z)^\top$. Again, the symmetric matrix $J(\nabla f_\sigma)$ will play a key role in the generalisation of MCM, self-snakes and active contours to 3×3 tensor data. We briefly sketch the adjustments that have to be made.

Mean Curvature Motion. In contrast to the 2×2 tensor case, we consider the two eigenvectors v, w corresponding to the two smallest eigenvalues of $J(\nabla f_\sigma)$. They determine the level surface parallel to which smoothing is allowed in a MCM-like process for 3×3 tensor data. The governing evolution equation for MCM reads then as

$$\begin{aligned} \partial_t u_{i,j} &= \partial_{vv} u_{i,j} + \partial_{ww} u_{i,j}, & (29) \\ u_{i,j}(x, y, z, 0) &= f_{i,j}(x, y, z) & (30) \end{aligned}$$

for the tensor channels (i, j) with $i, j = 1, 2, 3$.

Preservation of Positive Semidefiniteness. A number of tensor fields such as DT-MR images are positive semidefinite. Hence it would be desirable that an image processing method does not destroy this property. Let us now present a proof that twice differentiable solutions of MCM on the unbounded domain $\mathbb{R}^3 \times]0, +\infty[$ do preserve the positive semidefiniteness of the initial data. Under some additional technicalities one can expect that the reasoning below can also be extended to more general solution concepts such as viscosity solutions.
The tensor field $U(x, y, z, t) = (u_{i,j}(x, y, z, t))$ satisfying the evolution equation (29) is associated with the scalar-valued function representing the smallest eigenvalue $\lambda_{min}(x, y, z, t)$ of the matrix $U(x, y, z, t)$ at the point (x, y, z, t), and the well-known Rayleigh quotient

$$u^d(x, y, z, t) = d^\top U(x, y, z, t)\, d\,, \qquad (31)$$

where $d \in \mathbb{R}^3$ with $\|d\| = 1$. Let (x_0, y_0, z_0, t_0) be a local minimum of the function $\lambda_{\min}$. Due to the properties of the Rayleigh quotient we may choose a suitable eigenvector d to obtain

$$u^d(x_0, y_0, z_0, t_0) = \lambda_{\min}(x_0, y_0, z_0, t_0). \qquad (32)$$

We assumed in equation (29) that $v, w \in \mathbb{R}^3$ are the normalised eigenvectors of the structure tensor $J(\nabla u)$. Let us now consider the MCM evolution in the minimum point (x_0, y_0, z_0, t_0). The orthogonal vectors v and w are tangential

to the iso-surfaces of the tensor field. Due to the linearity of the differential operators involved, u^d satisfies

$$(u^d)_t = (u^d)_{vv} + (u^d)_{ww} \quad \text{for any } d \in \mathbb{R}^3. \tag{33}$$

A minimum is always a point of convexity, which implies for twice differentiable functions w that its Hessian $\mathrm{Hess}(w(x_0, y_0, t_0))$ is positive semidefinite. Hence in view of (32),(33) we have

$$\begin{aligned} \partial_t \lambda_{\min}(x_0, y_0, z_0, t_0) &= \partial_{vv} \lambda_{\min}(x_0, y_0, z_0, t_0) \\ &+ \partial_{ww} \lambda_{\min}(x_0, y_0, z_0, t_0) \\ &= v^\top \mathrm{Hess}(\lambda_{\min}(x_0, y_0, z_0, t_0))\, v \\ &+ w^\top \mathrm{Hess}(\lambda_{\min}(x_0, y_0, z_0, t_0))\, w \\ &\geq 0 \end{aligned} \tag{34}$$

since v and w represent the directions spanning the tangential plane to the iso-surface of the corresponding tensor field at the point (x_0, y_0, z_0, t_0). In other words: At a minimum point the smallest eigenvalue λ_{min} of the matrix in that point is *increasing in time*. This in turn implies preservation of positivity of the smallest eigenvalue. Hence the positive semidefiniteness of the initial tensor field is maintained.
It is evident that a corresponding proof is also valid in the 2×2 case. It can be found in [16].

Self-Snakes. The next curvature-based method to be extended to 3×3 tensor data is the self-snake PDE. Proceeding as in the 2×2 tensor case we obtain that its evolution is governed by the equation

$$\begin{aligned} \partial_t u_{i,j} &= g(\mathrm{tr} J(\nabla u_\sigma))\, \partial_{vv} u_{i,j} \\ &+ g(\mathrm{tr} J(\nabla u_\sigma))\, \partial_{ww} u_{i,j} \\ &+ \nabla^\top (g(\mathrm{tr} J(\nabla u_\sigma)))\, \nabla u_{i,j}, \end{aligned} \tag{35}$$

$$u_{i,j}(x, y, z, 0) = f_{i,j}(x, y, z). \tag{36}$$

As in the 2×2-tensor case the shock term $\nabla^\top (g(\mathrm{tr} J(\nabla u_\sigma)))\, \nabla u_{i,j}$ accounts for the edge-enhancing properties of this MCM variant.
With only minor modifications, it is possible to extend the semidefiniteness preservation proof for tensor-valued MCM also to the case of tensor-valued self-snakes. Since it does not provide additional insights, we do not present it here.

Active Contours. Finally, the geodesic active contour model carries over to the 3×3 setting via the scalar-valued equation

$$\begin{aligned} \partial_t u &= g(\mathrm{tr} J(\nabla h_\sigma))\, \partial_{vv} u \\ &+ g(\mathrm{tr} J(\nabla h_\sigma))\, \partial_{ww} u \\ &+ \nabla^\top (g(\mathrm{tr} J(\nabla h_\sigma)))\, \nabla u, \qquad (37) \\ u(x,y,z,0) &= f(x,y,z). \qquad (38) \end{aligned}$$

The evolving contour segments all 9 channels simultaneously making the process more noise resistant.

7 Numerical Implementation

Our implementation is based on explicit finite difference schemes for the two-dimensional evolutions (9), (19) and (24), as well as for their three-dimensional counterparts (29), (35) and (37). For computing the structure tensor of a matrix field, we replace the derivatives by central differences. Gaussian convolution is performed in the spatial domain with a sampled renormalised Gaussian K_σ that is truncated at $\pm 3\sigma$. Its symmetry and separability are used to accelerate the convolution. In the 2-D case the structure tensor is a 2×2 matrix, for which we compute its eigenvectors analytically. In the 3-D setting, the Jacobi method is used as a simple and robust strategy to obtain the eigenvectors numerically; see e.g. [45] for a detailed description.

The time derivative in the evolution PDEs is replaced by a forward difference. The discretisations of second order directional derivatives are based on the formulas

$$\begin{aligned} \partial_{vv} u &= v^\top \mathrm{Hess}(u)\, v, \qquad (39) \\ \partial_{ww} u &= w^\top \mathrm{Hess}(u)\, w, \qquad (40) \end{aligned}$$

where we approximate the second order spatial derivatives within the Hessian by central differences.

The shock terms of type $\nabla^\top g\, \nabla u$ involve first order spatial derivatives. In this case we use central differences for approximating ∇g and upwind discretisations for ∇u. For more details on upwind schemes for level set ideas we refer to [35].

It is difficult to establish strict stability bounds for discretisations of nonlinear curvature-based PDEs. In our experiments with explicit schemes we have observed stable behaviour for

$$\tau \left(\frac{1}{h_1^2} + \frac{1}{h_2^2} \right) \;\leq\; \frac{1}{2} \qquad (41)$$

in the 2-D case, and for

$$\tau \left(\frac{1}{h_1^2} + \frac{1}{h_2^2} + \frac{1}{h_3^2} \right) \leq \frac{1}{2} \tag{42}$$

in the 3-D case. Here τ denotes the time step size, and h_1, h_2 and h_3 are the grid sizes in x, y and z direction. These are the same stability restrictions as in the linear diffusion case with $\partial_t u = \Delta u$.

8 Experiments

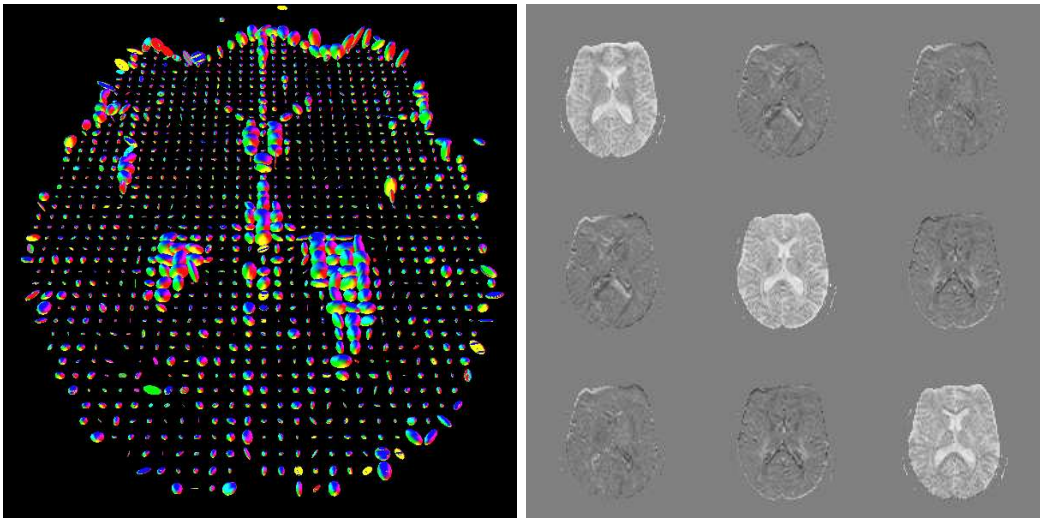

Figure 1: One slice of the 3-D DT-MRI data set which is used in the experiments. *Left:* Matrices represented by ellipsoids. Directions and lengths of the principle axes equal the eigenvectors and eigenvalues of the matrix. *Right:* Matrix components represented by grey-values. The 9 sub-images, each corresponding to one matrix entry, are arranged like the matrix entries. Because of the symmetry of the matrices, the three upper right sub-images appear again in the lower left part. Since all matrices are positive semidefinite, no negative values (darker than middle grey) appear in the main diagonal tiles.

The first test image we used for our experiments was obtained from a DT-MRI data set of a human brain. Its voxel size is $1.8mm \times 1.8mm \times 3mm$. For visualisation, we extract a 2-D section along the $x-y$ plane from the 3-D dataset. Figure 1 shows the 3×3 matrices from the selected 2-D section in two different ways: tensors as ellipsoids and a tile view. Note that while we are only showing the results in 2-D, data from all 3 dimensions have been used

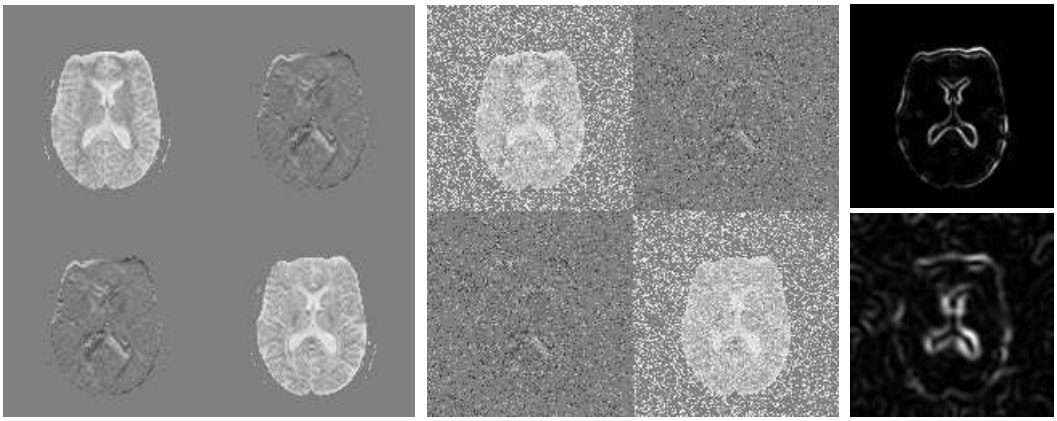

Figure 2: Edge detection with a structure tensor for matrix-valued data. (a) *Left:* Original 2-D tensor field extracted from the 3-D DT-MRI data set by using the channels $(1,1)$, $(1,2)$, $(2,1)$ and $(2,2)$. Each channel is of size 128×128. The channels $(1,2)$ and $(2,1)$ are identical for symmetry reasons. (b) *Middle:* Same image with 30 % noise. (c) *Top right:* Trace of the structure tensor of the original data. ($\sigma = 1.8$). (d) *Bottom right:* Trace of the structure tensor from the noisy image ($\sigma = 5.4$).

to compute these results. The tiled 2-D image consists of nine sub-images which show the nine tensor channels of a 3×3 matrix. Each channel has a resolution of 128×128 pixels. The top right off-diagonal channels and the bottom left off-diagonal channels are identical since the matrix is symmetric. To test the robustness under noise we have replaced 30 % of all data by noise matrices. Here, the eigenvector directions of the noise matrices are uniformly distributed on the unit sphere while the eigenvalues are uniformly distributed in the range which covers the data values themselves. We applied our methods to both the original image and the noisy image.
Figure 2 demonstrates the use of $\mathrm{tr}J(\nabla f_\sigma)$ for detecting edges in tensor-valued images. We observe that this method gives good results for the original data set. When increasing the noise scale σ, it is also possible to handle situations where massive noise is present.
Our second test image is a 2-D data set from fluid dynamics. It consists of 32×32 measurements. In each of these points a 2×2 matrix is given that describes the rate-of-deformation. As opposed to the first example, such matrices are indefinite, i.e. they have positive as well as negative eigenvalues. Figure 3 shows again the two alternative visualisations of the data by ellipsoids and in tiles. However, in this case the ellipsoids have to be understood as deformations of equally sized circles by directed contraction (for negative eigenvalues) or expansion (for positive eigenvalues).

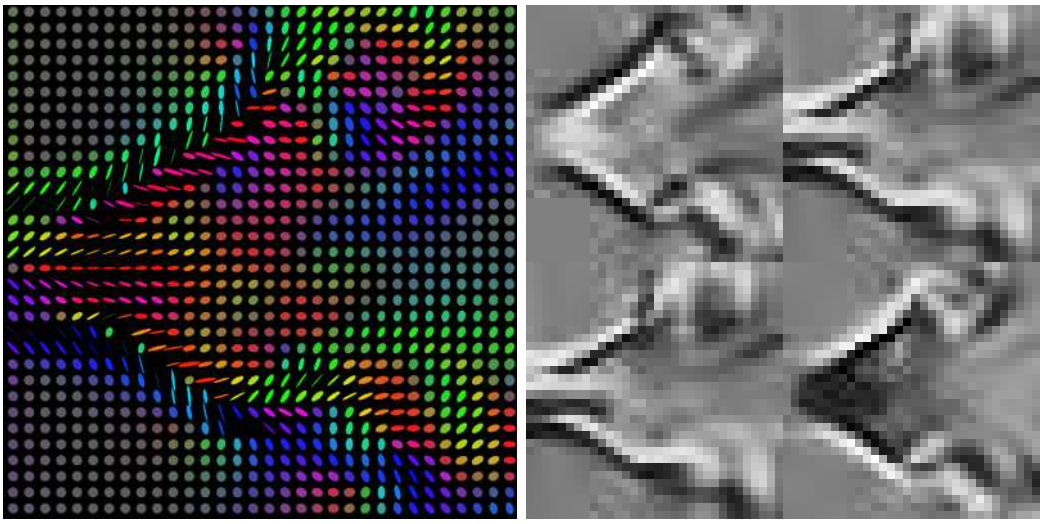

Figure 3: An image of size 32×32 containing indefinite 2×2 matrices. They describe the rate-of-deformation tensor in a fluid dynamics experiment. *Left:* Each matrix A is represented by an ellipse; directions and lengths of the principle axes equal eigenvectors and eigenvalues of $I + 0.5\,A$, where I is the unit matrix. Therefore a zero matrix is represented by a circle of radius 1. *Right:* Matrix components represented by grey-values. Again the symmetry implies equality between the upper right and lower left sub-image. However, the main diagonals here contain values of either sign.

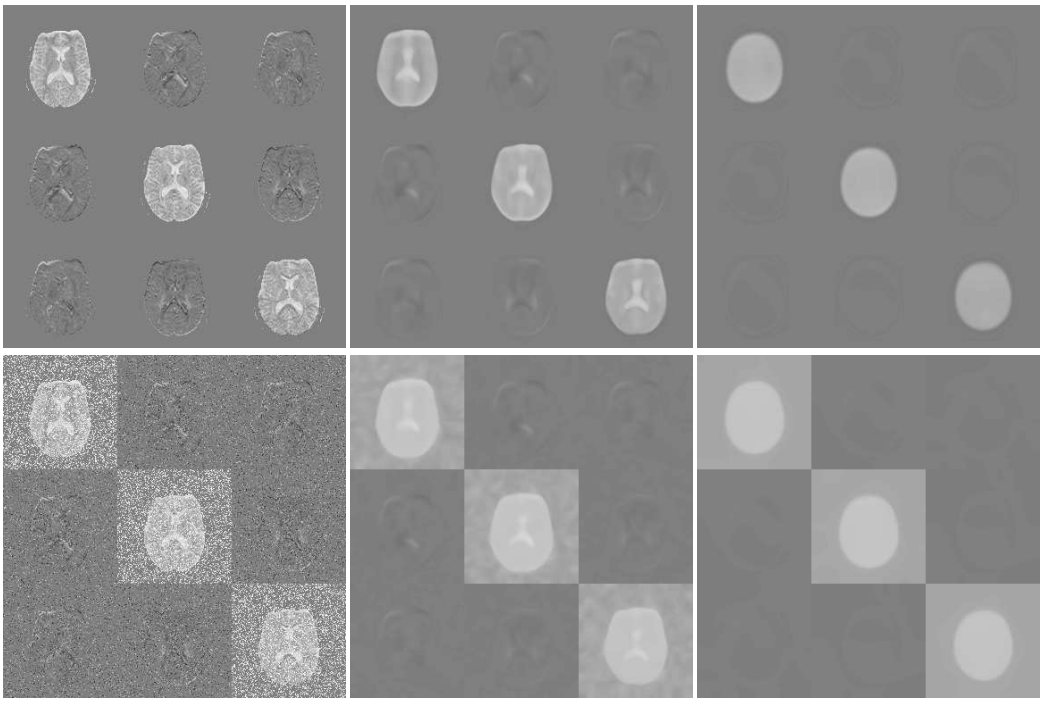

Figure 4: Tensor-valued 3-D mean curvature motion. *Top row, left to right:* One 128×128 slice from the original DT-MRI image, at time $t = 34$, at time $t = 340$. *Bottom row:* Same experiment with 30 % noise.

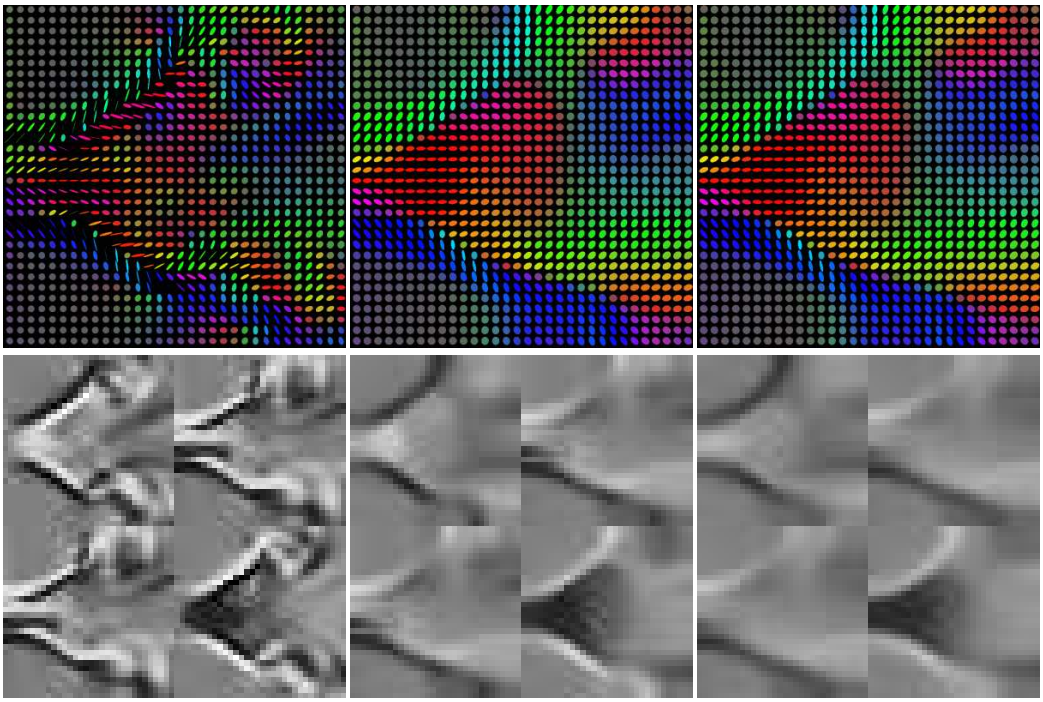

Figure 5: Tensor-valued 2D mean curvature motion. *Top, left to right:* The 32×32 fluid dynamics tensor image, its filtered version at time $t = 6.25$ and at time $t = 12.5$. *Bottom:* The same tensor fields shown as tiled grey-value images.

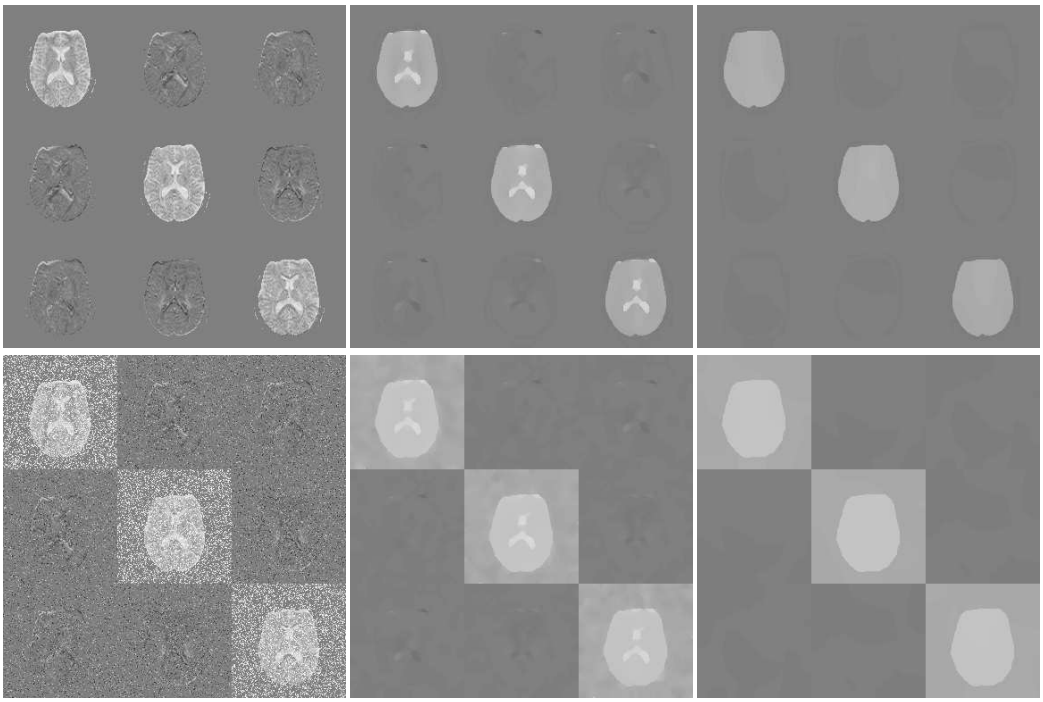

Figure 6: Tensor-valued 3-D self-snakes ($\sigma = 0.5$, $\lambda = 100$). *Top row, left to right:* One 128×128 slice from the original tensor image, at time $t = 136$, at time $t = 680$. *Bottom row:* Same experiment with 30 % noise.

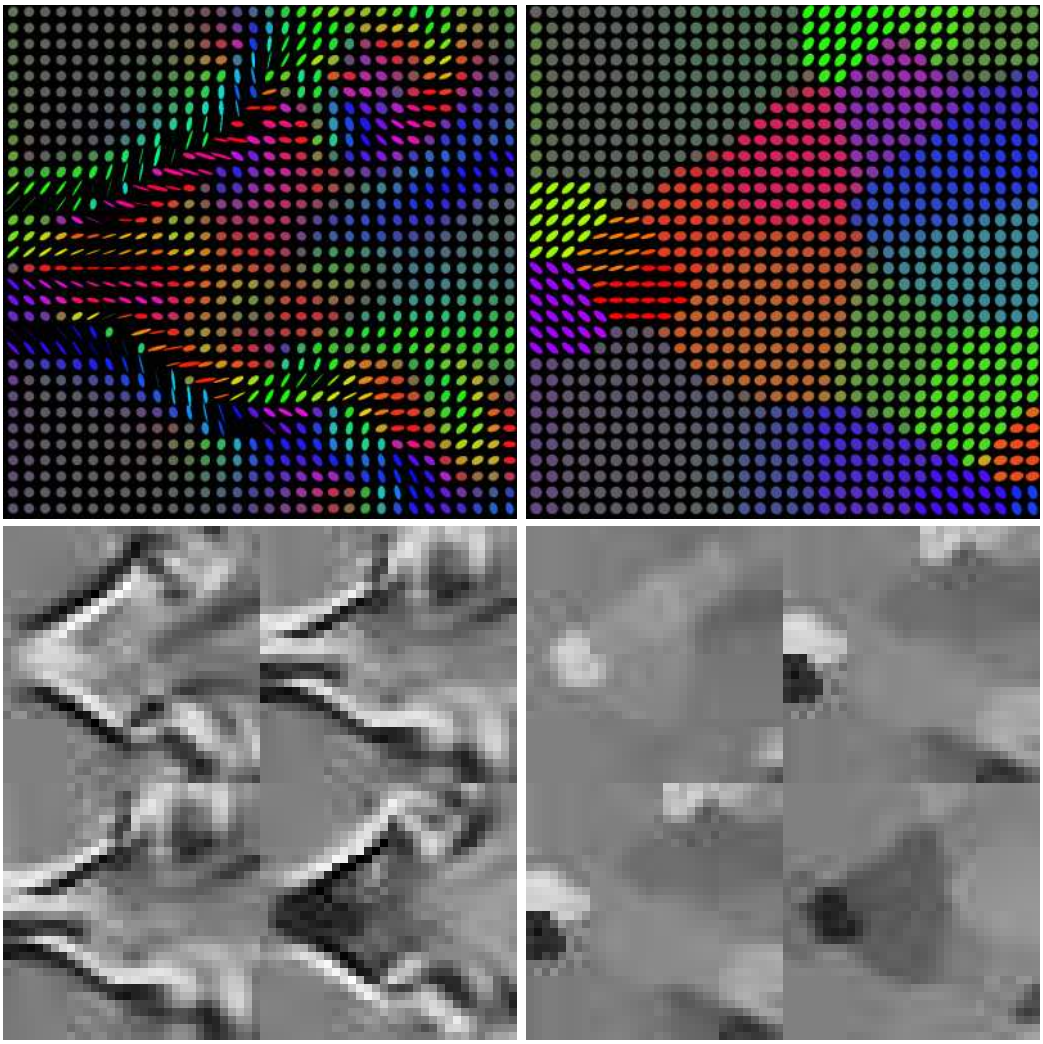

Figure 7: Tensor-valued 2D self-snakes. *Top left:* The 32×32 fluid dynamics tensor image. *Top right:* Filtered with $t = 25$, $\lambda = 0.05$, $\sigma = 0.5$. *Bottom:* Tiled grey-value view.

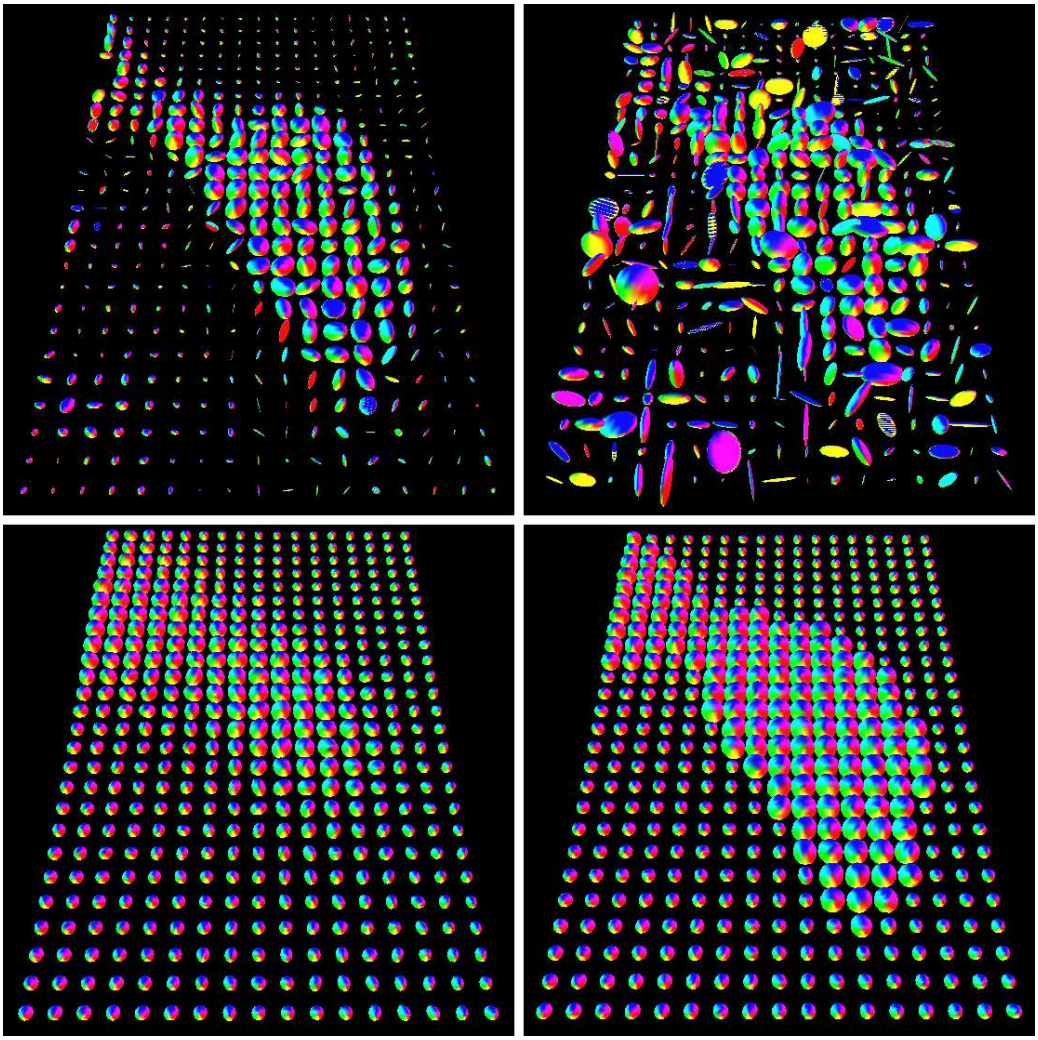

Figure 8: *Top left:* Detail from the 3-D DT-MRI brain dataset visualised by ellipsoids. The detail is taken from the slice shown in figures 4 and 6 and corresponds to the lower right part of the ventricle there. *Top right:* Same with 30 % of all matrices replaced by noise. *Bottom left:* The same image portion after applying 3-D MCM to the noisy image, $t = 34$. *Bottom right:* Same after self-snakes evolution, $t = 136$, $\sigma = 0.5$, $\lambda = 100$.

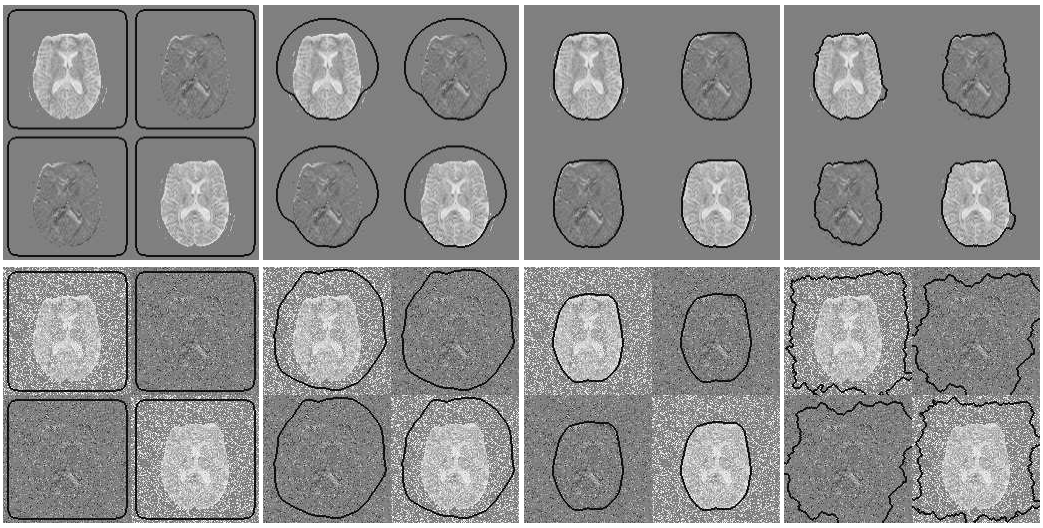

Figure 9: Tensor-valued geodesic active contours ($\sigma = 5.4$, $\lambda = 48.7$). *Top row, left to right:* Tensor image of size 128×128 including contour at time $t = 0$; $t = 3206.4$; $t = 32064$; uncoupled active contours at time $t = 32064$. *Bottom row:* Same experiments with 30 % noise.

In our next experiment we applied the tensor-valued mean curvature model to the three-dimensional DT-MRI data set. As can be seen in the first row of Figure 4, one experiences with scalar-valued mean curvature motion: Convex shapes shrink towards spheres before they vanish in finite time. This indicates that our method is a good extension to tensor-valued data. The second row of Figure 4 shows the same algorithm applied to the noisy image. As expected it possesses a high robustness to noise. Large evolution times give nearly identical results for the original and the noisy images, only the background in the noisy image turns lighter due to the noise.
Results of MCM evolution of the fluid dynamics tensor field are displayed in Figure 5. We observe that tensor-valued MCM has a strong tendency to simplify the streamlines. It may thus serve as an adequate scale-space representation for these type of images.
The results for the self-snake algorithm for three-dimensional tensor images are shown in Figures 6 and 7. They look similar to the three-dimensional MCM results, but they offer better sharpness at edges due to the additional shock term. It is also slowing down the evolution speed such that longer times are required for a similar image simplification. In general, tensor-valued self-snakes are preferable over tensorial MCM when one is interested in obtaining segmentation-like results.
Another comparison of MCM and self-snakes is depicted in Figure 8. Here

one can see a detail from the lower right part of the ventricle as shown in Figure 1. The tensors are visualised as ellipsoids and coloured according to the direction of their main axes. The shape is hardly detectable after applying 30 % of noise to the image. Evolving this image under MCM reveals this structure again, but the edges have softened considerably and the shape has shrunken in size. The self-snake method, on the other hand, shows the shape very clearly, with sharp and well-located edges.
Finally, we applied our active contour model to a 2-D tensor data set. In this case, we show a pure 2-D process. The 2×2 tensors consist exactly of the (1,1), (1,2), (2,1), (2,2) entries of the brain DT-MRI tensors from Figure 1. A 2-D version of the uniform noise described above was used to generate the noisy image. The goal was to extract the contour of the human brain shown on the original image. Figure 9 shows the temporal evolution of the active contours. First one notices that the evolution is slower in the noisy case. This is caused by the fact that noise creates large values in the trace of the structure tensor. This in turn slows down the evolution. For larger times, however, both results become very similar. This shows the high noise robustness of our active contour model for tensor-valued data sets. We contrast the result with the outcome of an uncoupled active contour model in the right column of Figure 9 to illustrate the superiority of the proposed channel coupling.

9 Summary and Conclusions

In this paper we have described how the scalar-valued PDE methods based on mean curvature motion, self-snakes and geodesic active contour models can be extended to tensor-valued data, both in the 2-D and the 3-D setting. This extension has been derived for the PDE-based approach as well as for its interpretation in terms of energy functionals. We have demonstrated that evolutions under tensor-valued mean curvature motion or tensor-valued self-snakes give positive semidefinite results for all positive semidefinite initial tensor fields. Experiments on positive semidefinite DT-MRI data and indefinite tensor fields from fluid dynamics illustrate that the proposed tensor-valued methods inherit characteristic properties of their scalar-valued counterparts. However, by using tensor-valued input data, they robustness under noise improves significantly. This is a consequence of the fact that all tensor channels simultaneously contribute to the calculation of the structure tensor that steers the process. As a result, curvature-driven PDEs appear even more attractive in the tensor setting than in the scalar framework. We hope that our paper serves as a starting point for investigating the numerous aspects

and applications of this promising class of tensor-valued methods in more detail.

Acknowledgments

We are grateful to Anna Vilanova i Bartrolí (Eindhoven Institute of Technology) and Carola van Pul (Maxima Medical Center, Eindhoven) for providing us with the DT-MRI data set and for discussing questions concerning data conversion. The fluid dynamics data set goes back to Prof. Wolfgang Kollmann (MAE Department, UC Davis) and has been kindly provided by Prof. Gerik Scheuermann (Institute for Informatics, University of Leipzig).

References

[1] L. Alvarez, P.-L. Lions, and J.-M. Morel. Image selective smoothing and edge detection by nonlinear diffusion. II. *SIAM Journal on Numerical Analysis*, 29:845–866, 1992.

[2] J. Bigün, G. H. Granlund, and J. Wiklund. Multidimensional orientation estimation with applications to texture analysis and optical flow. *IEEE Transactions on Pattern Analysis and Machine Intelligence*, 13(8):775–790, August 1991.

[3] T. Brox, M. Rousson, R. Deriche, and J. Weickert. Unsupervised segmentation incorporating colour, texture, and motion. In N. Petkov and M. A. Westenberg, editors, *Computer Analysis of Images and Patterns*, volume 2756 of *Lecture Notes in Computer Science*, pages 353–360. Springer, Berlin, 2003.

[4] T. Brox and J. Weickert. Nonlinear matrix diffusion for optic flow estimation. In L. Van Gool, editor, *Pattern Recognition*, volume 2449 of *Lecture Notes in Computer Science*, pages 446–453. Springer, Berlin, 2002.

[5] B. Burgeth, M. Welk, C. Feddern, and J. Weickert. Morphological operations on matrix-valued images. In T. Pajdla, J. Matas, and V. Hlaváč, editors, *Computer Vision – ECCV 2004*, Lecture Notes in Computer Science. Springer, Berlin, 2004. To appear.

[6] J. Campbell, K. Siddiqi, B. Vemuri, and G. B. Pike. A geometric flow for white matter fibre tract reconstruction. In *Proc. 2002 IEEE Interna-*

tional Symposium on Biomedical Imaging, pages 505–508, Washington, DC, July 2002.

[7] V. Caselles, F. Catté, T. Coll, and F. Dibos. A geometric model for active contours in image processing. *Numerische Mathematik*, 66:1–31, 1993.

[8] V. Caselles, R. Kimmel, and G. Sapiro. Geodesic active contours. In *Proc. Fifth International Conference on Computer Vision*, pages 694–699, Cambridge, MA, June 1995. IEEE Computer Society Press.

[9] V. Caselles, G. Sapiro, and D. H. Chung. Vector median filters, inf-sup convolutions, and coupled PDE's: theoretical connections. *Journal of Mathematical Imaging and Vision*, 12(2):109–119, April 2000.

[10] A. Chambolle. Partial differential equations and image processing. In *Proc. 1994 IEEE International Conference on Image Processing*, volume 1, pages 16–20, Austin, TX, November 1994. IEEE Computer Society Press.

[11] D. H. Chung and G. Sapiro. On the level lines and geometry of vector-valued images. *IEEE Signal Processing Letters*, 7(9):241–243, 2000.

[12] O. Coulon, D. C. Alexander, and S. A. Arridge. A regularization scheme for diffusion tensor magnetic resonance images. In M. F. Insana and R. M. Leahy, editors, *Information Processing in Medical Imaging – IPMI 2001*, volume 2082 of *Lecture Notes in Computer Science*, pages 92–105. Springer, Berlin, 2001.

[13] A. Cumani. Edge detection in multispectral images. *Graphical Models and Image Processing*, 53(1):40–51, 1991.

[14] A. Dervieux and F. Thomasset. A finite element method for the simulation of Rayleigh–Taylor instability. In R. Rautman, editor, *Approximation Methods for Navier–Stokes Problems*, volume 771 of *Lecture Notes in Mathematics*, pages 145–158. Springer, Berlin, 1979.

[15] S. Di Zenzo. A note on the gradient of a multi-image. *Computer Vision, Graphics and Image Processing*, 33:116–125, 1986.

[16] C. Feddern, J. Weickert, and B. Burgeth. Level-set methods for tensor-valued images. In O. Faugeras and N. Paragios, editors, *Proc. Second IEEE Workshop on Geometric and Level Set Methods in Computer Vision*, pages 65–72, Nice, France, October 2003. INRIA.

[17] M. Gage and R. S. Hamilton. The heat equation shrinking convex plane curves. *Journal of Differential Geometry*, 23:69–96, 1986.

[18] G. Gerig, O. Kübler, R. Kikinis, and F. A. Jolesz. Nonlinear anisotropic filtering of MRI data. *IEEE Transactions on Medical Imaging*, 11:221–232, 1992.

[19] G. H. Granlund and H. Knutsson. *Signal Processing for Computer Vision*. Kluwer, Dordrecht, 1995.

[20] M. Grayson. The heat equation shrinks embedded plane curves to round points. *Journal of Differential Geometry*, 26:285–314, 1987.

[21] F. Guichard and J.-M. Morel. Partial differential equations and image iterative filtering. In I. S. Duff and G. A. Watson, editors, *The State of the Art in Numerical Analysis*, number 63 in IMA Conference Series (New Series), pages 525–562. Clarendon Press, Oxford, 1997.

[22] K. Hahn, S. Pigarin, and B. Pütz. Edge preserving regularization and tracking for diffusion tensor imaging. In W. J. Niessen and M. A. Viergever, editors, *Medical Image Computing and Computer-Assisted Intervention – MICCAI 2001*, volume 2208 of *Lecture Notes in Computer Science*, pages 195–203. Springer, Berlin, 2001.

[23] G. Huisken. Flow by mean curvature of convex surfaces into spheres. *Journal of Differential Geometry*, 20:237–266, 1984.

[24] M. Kass, A. Witkin, and D. Terzopoulos. Snakes: Active contour models. *International Journal of Computer Vision*, 1:321–331, 1988.

[25] S. Kichenassamy, A. Kumar, P. Olver, A. Tannenbaum, and A. Yezzi. Gradient flows and geometric active contour models. In *Proc. Fifth International Conference on Computer Vision*, pages 810–815, Cambridge, MA, June 1995. IEEE Computer Society Press.

[26] B. B. Kimia and K. Siddiqi. Geometric heat equation and non-linear diffusion of shapes and images. *Computer Vision and Image Understanding*, 64:305–322, 1996.

[27] R. Kimmel. *Numerical Geometry of Images: Theory, Algorithms, and Applications*. Springer, New York, 2003.

[28] H. P. Kramer and J. B. Bruckner. Iterations of a non-linear transformation for enhancement of digital images. *Pattern Recognition*, 7:53–58, 1975.

[29] Z. Krivá and K. Mikula. An adaptive finite volume method in processing of color images. In *Proc. Algoritmy 2000 Conference on Scientific Computing*, pages 174–187, Podbanské, Slovakia, September 2000.

[30] R. Malladi, J. A. Sethian, and B. C. Vemuri. A topology independent shape modeling scheme. In B. Vemuri, editor, *Geometric Methods in Computer Vision*, volume 2031 of *Proceedings of SPIE*, pages 246–258. SPIE Press, Bellingham, 1993.

[31] G. Medioni, M.-S. Lee, and C.-K. Tang. *A Computational Framework for Segmentation and Grouping*. Elsevier, Amsterdam, 2000.

[32] S. Osher and R. P. Fedkiw. *Level Set Methods and Dynamic Implicit Surfaces*, volume 153 of *Applied Mathematical Sciences*. Springer, New York, 2002.

[33] S. Osher and N. Paragios, editors. *Geometric Level Set Methods in Imaging, Vision and Graphics*. Springer, New York, 2003.

[34] S. Osher and L. I. Rudin. Feature-oriented image enhancement using shock filters. *SIAM Journal on Numerical Analysis*, 27:919–940, 1990.

[35] S. Osher and J. A. Sethian. Fronts propagating with curvature-dependent speed: Algorithms based on Hamilton–Jacobi formulations. *Journal of Computational Physics*, 79:12–49, 1988.

[36] G. J. M. Parker, J. A. Schnabel, M. R. Symms, D. J. Werring, and G. J. Barker. Nonlinear smoothing for reduction of systematic and random errors in diffusion tensor imaging. *Journal of Magnetic Resonance Imaging*, 11:702–710, 2000.

[37] P. Perona and J. Malik. Scale space and edge detection using anisotropic diffusion. *IEEE Transactions on Pattern Analysis and Machine Intelligence*, 12:629–639, 1990.

[38] C. Pierpaoli, P. Jezzard, P. J. Basser, A. Barnett, and G. Di Chiro. Diffusion tensor MR imaging of the human brain. *Radiology*, 201(3):637–648, December 1996.

[39] C. Poupon, J.-F. Mangin, V. Frouin, J. Régis, F. Poupon, M. Pachot-Clouard, D. Le Bihan, and I. Bloch. Regularization of MR diffusion tensor maps for tracking brain white matter bundles. In W. M. Wells, A. Colchester, and S. Delp, editors, *Medical Image Computing and Computer-Assisted Intervention – MICCAI 1998*, volume 1496 of *Lecture Notes in Computer Science*, pages 489–498. Springer, Berlin, 1998.

[40] T. Preußer and M. Rumpf. A level set method for anisotropic geometric diffusion in 3D image processing. *SIAM Journal on Applied Mathematics*, 62(5):1772–1793, 2002.

[41] A. R. Rao and B. G. Schunck. Computing oriented texture fields. *CVGIP: Graphical Models and Image Processing*, 53:157–185, 1991.

[42] G. Sapiro. Vector (self) snakes: a geometric framework for color, texture and multiscale image segmentation. In *Proc. 1996 IEEE International Conference on Image Processing*, volume 1, pages 817–820, Lausanne, Switzerland, September 1996.

[43] G. Sapiro. *Geometric Partial Differential Equations and Image Analysis*. Cambridge University Press, Cambridge, UK, 2001.

[44] G. Sapiro and D. L. Ringach. Anisotropic diffusion of multivalued images with applications to color filtering. *IEEE Transactions on Image Processing*, 5(11):1582–1586, 1996.

[45] H. R. Schwarz. *Numerical Analysis: A Comprehensive Introduction*. Wiley, New York, 1989.

[46] J. A. Sethian. *Level Set Methods and Fast Marching Methods*. Cambridge University Press, Cambridge, UK, second edition, 1999.

[47] X. Tricoche, G. Scheuermann, and H. Hagen. Vector and tensor field topology simplification on irregular grids. In D. Ebert, J. M. Favre, and R. Peikert, editors, *Proc. Joint Eurographics – IEEE TCVG Symposium on Visualization*, pages 107–116. Springer, Wien, 2001.

[48] D. Tschumperlé and R. Deriche. Orthonormal vector sets regularization with PDE's and applications. *International Journal of Computer Vision*, 50(3):237–252, December 2002.

[49] D. Tschumperlé and R. Deriche. Vector-valued image regularization with PDE's: a common framework for different applications. In *Proc. 2003 IEEE Computer Society Conference on Computer Vision and Pattern Recognition*, volume 1, pages 651–656, Madison, WI, June 2003. IEEE Computer Society Press.

[50] B. Vemuri, Y. Chen, M. Rao, T. McGraw, Z. Wang, and T. Mareci. Fiber tract mapping from diffusion tensor MRI. In *Proc. First IEEE Workshop on Variational and Level Set Methods in Computer Vision*, pages 73–80, Vancouver, Canada, July 2001. IEEE Computer Society Press.

[51] Z. Wang and B. C. Vemuri. An affine invariant tensor dissimilarity measure and its applications to tensor-valued image segmentation. In *Proc. 2004 IEEE Computer Society Conference on Computer Vision and Pattern Recognition*, Washington, DC, June 2004. IEEE Computer Society Press. In press.

[52] J. Weickert. Coherence-enhancing diffusion of colour images. *Image and Vision Computing*, 17(3–4):199–210, March 1999.

[53] J. Weickert and T. Brox. Diffusion and regularization of vector- and matrix-valued images. In M. Z. Nashed and O. Scherzer, editors, *Inverse Problems, Image Analysis, and Medical Imaging*, volume 313 of *Contemporary Mathematics*, pages 251–268. AMS, Providence, 2002.

[54] M. Welk, C. Feddern, B. Burgeth, and J. Weickert. Median filtering of tensor-valued images. In B. Michaelis and G. Krell, editors, *Pattern Recognition*, volume 2781 of *Lecture Notes in Computer Science*, pages 17–24, Berlin, 2003. Springer.

[55] C.-F. Westin, S. E. Maier, B. Khidhir, P. Everett, F. A. Jolesz, and R. Kikinis. Image processing for diffusion tensor magnetic resonance imaging. In C. Taylor and A. Colchester, editors, *Medical Image Computing and Computer-Assisted Intervention – MICCAI 1999*, volume 1679 of *Lecture Notes in Computer Science*, pages 441–452. Springer, Berlin, 1999.

[56] R. T. Whitaker and X. Xue. Variable-conductance, level-set curvature for image denoising. In *Proc. 2001 IEEE International Conference on Image Processing*, pages 142–145, Thessaloniki, Greece, October 2001.

[57] L. Zhukov, K. Munseth, D. Breen, R. Whitaker, and A. H. Barr. Level set modeling and segmentation of DT-MRI brain data. *Journal of Electronic Imaging*, 12(1):125–133, 2003.